Received: 29 May 2017 | Revised: 3 January 2018 | Accepted: 8 January 2018

DOI: 10.1002/hipo.22830

RESEARCH ARTICLE

WILEY

Parvalbumin interneuron mediated feedforward inhibition controls signal output in the deep layers of the perirhinal-entorhinal cortex

Janske G. P. Willems | Wytse J. Wadman | Natalie L. M. Cappaert

Center for Neuroscience, Sammerdam Institute for Life Sciences, University of Amsterdam, SciencePark 904, Amsterdam 1098 XH, The Netherlands

Correspondence
N. L. M. Cappaert, PhD, Swammerdam Institute for Life Sciences, Center for Neuroscience, University of Amsterdam, The Netherlands.
Email: N.Cappaert@uva.nl

Abstract

The perirhinal (PER) and lateral entorhinal (LEC) cortex form an anatomical link between the neocortex and the hippocampus. However, neocortical activity is transmitted through the PER and LEC to the hippocampus with a low probability, suggesting the involvement of the inhibitory network. This study explored the role of interneuron mediated inhibition, activated by electrical stimulation in the agranular insular cortex (AiP), in the deep layers of the PER and LEC. Activated synaptic input by AiP stimulation rarely evoked action potentials in the PER-LEC deep layer excitatory principal neurons, most probably because the evoked synaptic response consisted of a small excitatory and large inhibitory conductance. Furthermore, parvalbumin positive (PV) interneurons—a subset of interneurons projecting onto the axo-somatic region of principal neurons—received synaptic input earlier than principal neurons, suggesting recruitment of feedforward inhibition. This synaptic input in PV interneurons evoked varying trains of action potentials, explaining the fast rising, long lasting synaptic inhibition received by deep layer principal neurons. Altogether, the excitatory input from the AiP onto deep layer principal neurons is overruled by strong feedforward inhibition. PV interneurons, with their fast, extensive stimulus-evoked firing, are able to deliver this fast evoked inhibition in principal neurons. This indicates an essential role for PV interneurons in the gating mechanism of the PER-LEC network.

KEYWORDS

excitation/inhibition balance, mouse, patch clamp, parahippocampal region, pyramidal neurons

1 | INTRODUCTION

The perirhinal (PER) and the lateral entorhinal (LEC) cortex are both involved in processing object information in the so called "what" pathway (Eichenbaum, Sauvage, Fortin, Komorowski, & Lipton, 2012; van Strien, Cappaert, & Witter, 2009; Witter, Groenewegen, Lopes da Silva, & Lohman, 1989). The PER and LEC receive afferent projections from the agranular insular cortex (AiP) (Burwell, 2000; Mathiasen, Hansen, & Witter, 2015), a neocortical area involved in emotional, interoceptive, and exteroceptive signal processing (Nieuwenhuys, 2012). In turn, PER and LEC axons project to the hippocampal formation (for review see Witter, 1993). Although there are anatomical projections present to convey information from the neocortex, through the PER and LEC, to the hippocampal formation, neuronal activity is not reliably transmitted through this network (Biella, Uva, & de Curtis, 2002; Pelletier, Apergis, & Paré, 2004; Willems, Wadman, & Cappaert, 2016). This suggests that the PER-LEC network, instead of simply acting as a relay station, actively selects and processes information (de Curtis & Paré, 2004).

Still, the neuronal mechanism behind these selecting and processing capabilities is not fully understood. It is shown though, that principal neurons in both the PER and LEC network stop firing up to 300 ms when a cortical input is received (Pelletier et al., 2004). This suppression presumably originates from inhibitory interneurons as reducing the inhibition by partly antagonizing the $GABA_A$ receptor activity resulted

in reliable transmission of neocortical synaptic input, implying a role for GABAergic interneurons in controlling relay of activity in the PER-LEC network (Koganezawa et al., 2008; Willems et al., 2016).

Previous studies also showed that a stimulus in the local PER-LEC network evoked inhibitory as well as excitatory responses, whereas a distal stimulus resulted mainly in excitation (Biella, Uva, & Curtis, 2001; Martina, Royer, & Paré, 2001). This suggests that inhibition is mainly recruited in the local circuitry (Unal, Pare, Smith, & Pare, 2013). An ultrastructural study revealed that the GABAergic neurons are presumably organized in a feed-forward manner (Pinto, Fuentes, & Paré, 2006). The origin of the functional inhibition in the PER-LEC network is still needs to be determined.

Potential candidates for efficient inhibitory control of principal neurons are parvalbumin positive (PV) interneurons (Pfeffer, Xue, He, Huang, & Scanziani, 2013). This interneuron type is present in all layers of the PER and even more abundantly in the LEC (Wouterlood, Härtig, Brückner, & Witter, 1995). PV interneurons are known for their high-frequency firing capabilities and they project onto the axo-somatic region of principal neurons. Hence, PV interneurons are capable of strongly regulating principal neuron output by shaping oscillatory activity (Cunningham et al., 2006; Sohal, Zhang, Yizhar, & Deisseroth, 2009). Loss of inhibition in the PER-LEC is associated with pathologies involving hyperexcitability such as temporal lobe epilepsy and psychiatric illness (Cunningham et al., 2006; Kumar & Buckmaster, 2006). Furthermore, PV interneuron numbers decrease tremendously in the PER of epileptic rats (Biagini et al., 2013) and PV interneuron activation can terminate epileptic activity in the mouse model for epilepsy (Assaf & Schiller, 2016).

This study investigated whether the interplay between principal neurons and PV interneurons performs a role in processing of synaptic input to the deep layers of the PER-LEC network. We examined the stimulus evoked synaptic input and action potential firing patterns in principal neurons and PV interneurons to address the functional output of the PER-LEC network once synaptic input is processed in the local circuitry.

2 | MATERIALS AND METHODS

2.1 | Animals

Experiments were performed on 22 male and female C57Bl/6 mice (Harlan Netherlands BV, Horst) and 18 male and female Pvalb$^{tm1(cre)Arbr}$ (Hippenmeyer et al., 2005)/Gt(ROSA)26Sor$^{tm1(EYFP)Cos}$ (Srinivas et al., 2001) (PV/YFP) transgenic mice. Experiments to confirm the reversal potential for fast, chloride mediated inhibition were performed on 4 Pvalb$^{tm1(cre)Arbr}$/Gt(ROSA)26Sor$^{tm32(CAG-COP4*H134R/EYFP)Hze}$ (Madisen et al., 2012) transgenic mice. All animals were between the ages of P28 and P42. Animal care and experiments were approved by the Animal Care and Use committee of the University of Amsterdam and were in accordance with European guidelines.

2.2 | Slice preparation

Animals were killed by decapitation, whereafter the brain was rapidly removed and stored in ice-cold modified artificial cerebrospinal fluid (mACSF) containing (in mM): 120 choline chloride, 3.5 KCl, 5 $MgSO_4$, 1.25 NaH_2PO_4, .5 $CaCl_2$, 25 $NaHCO_3$, 10 D-glucose (pH 7.4, 300–315 mOsmol), oxygenated with 95% O_2/5% CO_2 for at least 30 min. Horizontal slices (400 μm thick) containing the neocortical AiP, PER, and LEC (Figure 1e) (Willems et al., 2016) were cut in ice-cold mACSF using a VT1200S vibratome (Leica Biosystems, Nussloch, Germany). Functional projections from the AiP to the PER and EC are present in this slice preparation (von Bohlen und Halbach & Albrecht, 2002; Mathiasen et al., 2015; Willems et al., 2016). After sectioning, slices were incubated in ACSF containing (in mM): 120 NaCl, 3.5 KCl, 1.3 $MgSO_4$, 1.25 NaH_2PO_4, 2.5 $CaCl_2$, 25 $NaHCO_3$, 10 D-glucose, oxygenated with 95% O_2/5% CO_2 (pH 7.4, 300–315 mOsmol) at 32 °C for 15 min, thereafter slices were kept at room temperature until the recording started.

2.3 | Whole cell recordings in principal neurons

In total 81 principal neurons were recorded in the PER and LEC deep layers. The localization of the PER and LEC in our slice preparation was based on the mouse brain atlas (Paxinos & Franklin, 2001). Patch pipettes were pulled using micropipette puller model P-87 (Sutter Instrument, Novato, CA) and had a resistance of 3–5 MΩ. Whole-cell recordings were performed using an intracellular solution containing (in mM): 131.25 K-gluconate, 8.75 KCl, 10 HEPES, .5 EGTA, 4 MgATP, .4 Na2GTP, pH adjusted to 7.4, 295–300 mOsmol. 1% biocytin (Sigma-Aldrich, Saint Louis, MO) was added to the intracellular solution for post hoc visualization and morphological identification of the recorded neuron. During the recordings, slices were perfused with ACSF of 30 °C at a rate of 2 mL/min. Deep layer PER and LEC principal neurons were selected based on large soma size using a Scientifica SliceScope Pro 6000 (Scientifica, Uckfield, UK). Whole-cell recordings were made using an Axopatch 200B amplifier (Molecular Devices, Sunnyvale, CA), filtered at 10 kHz, sampled at 100 kHz and digitized using a NI DAQ usb-6259 (National Instruments, Austin, TX). Software for data-acquisition was custom made in MatLab (MathWorks, Natick, MA). All voltage signals were corrected online for a −14 mV junction potential. Principal neurons were approached with slight pressure on the pipette and when pressure was released the pipet-cell contact had to reach a seal of 1 GΩ before break in. Immediately after break in, the resting membrane potential was recorded in current clamp at a 0 pA holding current. Access resistance was compensated for at least 50–60% and recordings with an access resistance higher than 20 MΩ or with more than 25% change during the recording were discarded.

In some experiments, the glutamatergic transmission was blocked by bath application of 20 μM AMPA receptor antagonist CNQX (Abcam, Cambridge, UK) and 10 μM NMDA receptor antagonist APV (Tocris, Bristol, UK). All other chemicals were obtained from Sigma-Aldrich (Saint-Louis, MO).

2.4 | Electrical stimulation

For electrical stimulation, a bipolar tungsten stimulus electrode (World Precision Instruments, Sarasota, FL) with a tip separation of 125 μm was placed under visual guidance in the superficial layers of the AiP. A single bi-phasic stimulus pulse (160 μs/phase) was

applied using a DS4 bi-phasic current stimulator (Digitimer Ltd, Hertfordshire, UK).

2.5 | Data analysis

The response latency, defined as the onset of an EPSC, EPSP or an excitatory or inhibitory conductance, was determined as the time difference between the stimulus and the point where the signal exceeded 8 times the baseline standard deviation, within 75 ms after the stimulus was applied. If a response latency was detected the peak and the half width of the response were determined. The peak of the response was characterized as the maximum amplitude after the onset latency and the half width was defined as the time between the point where the response crosses the 50% of the maximum response before and after the peak.

The peak and peak time of the action potentials was determined using Matlab (peakdet function), to address the presence and rate of action potential firing.

2.6 | Decomposition of stimulus evoked synaptic currents

The evoked synaptic response in a neuron contains components that originate from excitatory and inhibitory synapses. As blocking some of these components with pharmaceuticals will affect all responses in the network, we linearly decomposed the current into two underlying components that have a different reversal potential. The postsynaptic cell was clamped at potentials between −90 mV and −50 mV, while evoking the same, voltage-independent, synaptic conductance (see inset in Figure 3b,c). After subtraction of the stimulus independent background current, this results in a membrane current that contains the excitatory synaptic current and the inhibitory synaptic current:

$$I_m(t) = I_{exc}(t) + I_{inh}(t)$$

These currents are the result of the excitatory and the inhibitory synaptic conductances ($G_{exc}(t)$ and $G_{inh}(t)$) and their respective driving forces, being the differences between membrane voltage V_m and the excitation and inhibition reversal potentials (E_{exc} and E_{inh}):

$$I_m(t) = G_{exc}(t)(V_m(t) - E_{exc}) + G_{inh}(t)(V_m(t) - E_{inh})$$

The instantaneous relation between membrane current and membrane can, at each moment in time, be summarized by:

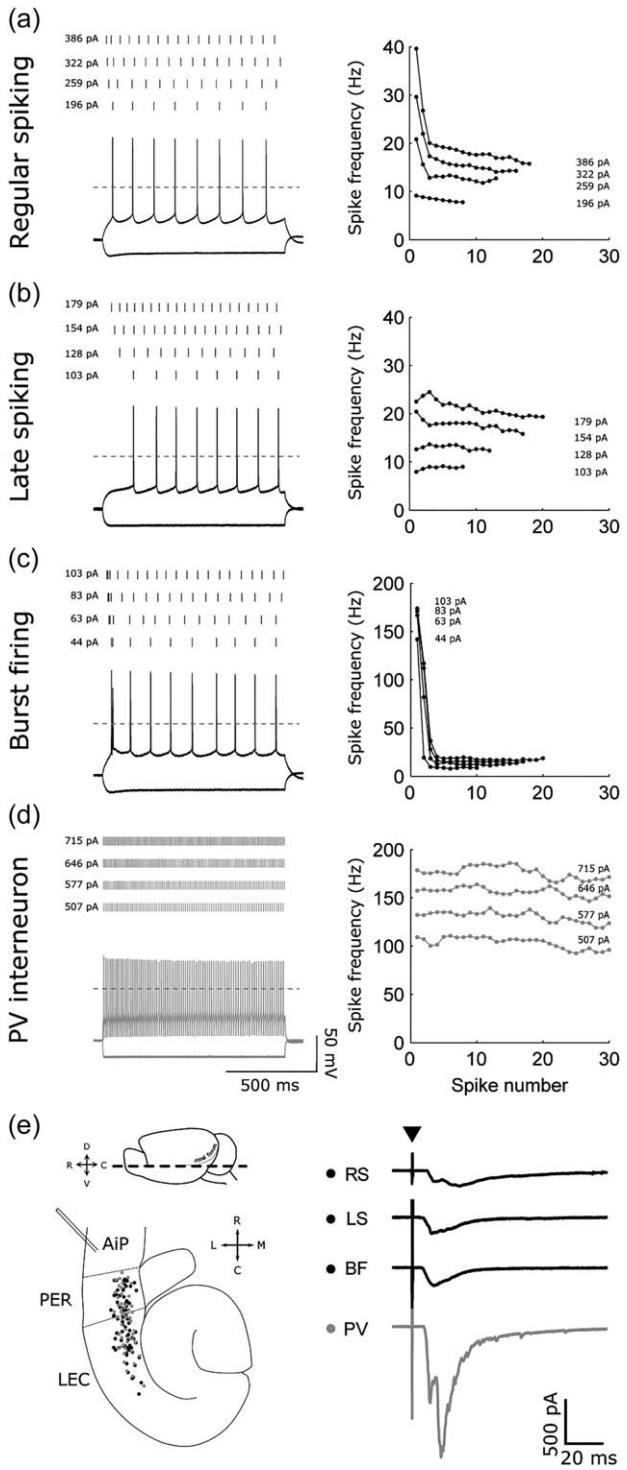

FIGURE 1.

FIGURE 1 Intrinsic properties of three types of principal neurons and PV positive interneurons in the PER-LEC deep layer network. Typical example of the spike pattern (left), and spike-frequency plot (right) of regular spiking (a), late spiking (b), and burst firing (c) principal neurons and PV positive interneurons (d, gray). (a–d left) Top: spike raster plot of four current injections of increasing amplitudes. Bottom: membrane voltage in response to a hyperpolarizing and threshold depolarizing current injection. (a–d right) Spike-frequency of every spike at four current injections of increasing amplitudes. (e) Left top: schematic representation of the lateral view of the mouse brain, the dotted line indicates the slice location. Left bottom: Representation of the distribution of the three principal neuron types (black) and PV interneurons (gray) recorded in a schematic horizontal mouse brain slice containing the AiP as the stimulated neocortical area, the PER and LEC. Right: Evoked synaptic currents in response to AiP stimulation in three classes of principal neurons (black), that is, RS, LS, BF neurons, and PV interneurons (gray). The responses are from the same neurons as shown in a–d. The arrowhead (▼) indicates the moment the stimulus was applied. Abbreviations: PER, perirhinal cortex; LEC, lateral entorhinal cortex; R, rostral; C, caudal; L, lateral; M, medial; RS, regular spiking; LS, late spiking; BF, burst firing; PV, parvalbumin

$$I_m = (G_{exc} + G_{inh}) * V_m - (G_{exc} * E_{exc} + G_{inh} * E_{inh})$$

The last equation is the linear I/V relation $I_m = a * V_m + b$, which can be calculated at each moment in time and from which the time varying conductances can now be constructed:

$$G_{inh}(t) = (b(t) + a(t) * E_{exc}) / (E_{exc} - E_{inh})$$

$$G_{exc}(t) = \left(a(t) - G_{inh(t)}\right)$$

We performed this calculation for 100 ms after the stimulus and with .1 ms time resolution. If there are only glutamatergic and $GABA_A$ergic synapses activated and we have exact knowledge of their (time-invariant) reversal potentials (0 mV, respectively, −70 mV) (Melzer et al., 2012; Purves et al., 2001), G_{exc} and G_{inh} describe the time course of the synaptic conductances in the cell. The reversal potential of the fast, $GABA_A$ mediated inhibition was verified in slices from transgenic mice expressing the light activated channelrhodopsin (ChR2) specifically in PV interneurons. Optical activation of ChR2 in PV interneurons depolarized the PV interneurons and evoked action potential firing. In this way, we specifically induced PV related IPSCs in the postsynaptic principal cells and calculated the reversal potential of that component, revealing the E_{inh} (−70.2 ± .4 mV, $n = 30$ IPSCs in two principal neurons; data not shown). This value, together with the well-established value of 0 mV for the E_{exc} was used for the decomposition. The conductances induced by AiP stimulation were averaged over three repetitions.

2.7 | Paired whole cell recordings of principal neurons and PV interneurons

PV expressing interneurons in the PER and LEC network were identified using transgenic mice conditionally expressing YFP driven by the PV promotor dependent cre-recombinase expression (Supporting Information Figure 1d). YFP was excited at 470 nm using LED illumination light source (PE-100,CoolLed Ltd., Andover, UK) and a 479 ± 40 nm emission filter (Thorlabs Inc., Newton NJ). Paired whole-cell recordings of one PV interneuron and one principal neuron were performed with a maximal intersoma distance of 200 μm. The firing properties of the cells were recorded by injecting a membrane current that set the membrane voltage from −100 to −30 mV in steps of 5–10 mV. Connectivity between the principal neuron and PV interneuron was tested by evoking action potentials in the principal neuron at reproducible random moments using a frozen noise current injection (Zeldenrust, Chameau, & Wadman, 2013) and recording unitary excitatory postsynaptic currents (uEPSCs) in the PV interneurons clamped at −70 mV (Figure 6a). We strived to induce a firing rate of 1–2 Hz in the principal neuron. The reversed configuration was used to establish PV to principal neuron connectivity, holding the principal cell at −50 mV to record unitary inhibitory postsynaptic currents (uIPSCs; Figure 6b).

Next, we addressed the stimulus-evoked synaptic current in voltage clamp (−70 mV) and action potential firing in current clamp in response to AiP stimulation in both principal neuron and PV interneuron. The maximum stimulus intensity was 836 ± 43 μA, we adjusted the stimulation strength on the response of the principal neuron. Subsequently, evoked synaptic currents were recorded at five holding potentials (−90 to −50 mV) in the principal neuron and PV firing was recorded in current clamp at the same time to compare the estimated evoked inhibitory conductance in the principal neuron to the spiking of PV neurons.

2.8 | Histology

For visualization of the recorded neurons, slices were fixed in 4% PFA in PBS overnight at 4 °C after the recording. After 5 washes in PBS (10 min each), sections were permeabilized with .25% Triton in PBS and biocytin was labeled using Streptavidin-Alexa 488 conjugate (Sigma-Aldrich, Saint Louis, MO) 1:200 diluted in .25% Triton in PBS, incubated overnight at 4 °C. After staining, slices were washed in PBS and mounted in Vectashield (Vector Laboratories Inc., Burlingame, CA). Biocytin filled neurons were visualized using an A1 confocal microscope (Nikon Instruments Europe, Amsterdam, The Netherlands) and their morphology was further examined in ImageJ (Schindelin, Rueden, Hiner, & Eliceiri, 2015; Schindelin et al., 2012).

For the verification of YFP expression specifically in PV interneurons in PV/YFP mice, brains were removed like the above procedure and fixed in 4% PFA in PBS for 8 hr at 4 °C. After fixation, brains were placed in 15% sucrose in PBS for 2 hr and in 30% sucrose in PBS until submerged for cryoprotection. Brains were snap frozen in dry ice and 40 μm cryosections were made and slices were kept free floating in antifreeze at −20 °C. For immunostaining, slices were rinsed in PBS and blocked with 10% normal donkey serum in .4% Triton in PBS for 1 hr. Subsequently, slices were incubated with the primary antibodies Rabbit-anti-PV (ab11427, Abcam, Cambridge, UK) and anti-GFP-488 conjugated (A21311, Invitrogen, Carlsbad, CA) to visualize YFP expression. The primary Rabbit-anti-PV antibody was visualized by a Donkey-anti-Rabbit-Cy3 secondary antibody (Jackson ImmunoResearch Laboratories, West Grove, PA). Cell nuclei were counterstained with Hoechst 33258 (H3569, ThermoFisher Scientific, Waltham, MA).

2.9 | Statistics

All values are reported as mean and standard error of the mean (*SEM*). Statistical analysis was performed using Matlab or Prism 6 (Graphpad Software Inc., La Jolla, CA). Unless otherwise mentioned, pairwise comparisons were made using Student's *t*-test; multiple comparisons were performed using ANOVA with the appropriate post hoc tests and correlations were analyzed using linear regression. $p < .05$ was assumed to reject the null hypothesis.

3 | RESULTS

3.1 | Three classes of principal neurons in the per-LEC deep layers

Whole cell recordings of 81 deep layer principal neurons in horizontal mouse brain slices were performed. Deep layer principal neurons were identified by their physiological properties and postrecording visualization of their localization, that is, pyramidal like cell body and basal dendrites in the deep layers (Canto & Witter, 2012; Hamam, Amaral, & Alonso, 2002). Intrinsic membrane properties and action potential firing

TABLE 1 Intrinsic properties of principal neurons and PV interneurons

Property	RS neurons ($n = 58$)	LS neurons ($n = 11$)	BF neurons ($n = 12$)	PV interneurons ($n = 63$)
RMP (mV)	−63.5 ± .5	−64.9 ± 1.2	−63.8 ± 1.3	−65.7 ± .5
Input resistance (MΩ)	105 ± 6	130 ± 9	171 ± 19	110 ± 5
Membrane τ (ms)	8.7 ± .4	6.9 ± .7	8.3 ± .5	4.4 ± .1
Sag (mV)	−2.4 ± .2	–.7 ± .1	−2.5 ± .4	–.4 ± .1
Time to first AP (ms)	59 ± 3	143 ± 13	46 ± 7	25 ± 5
AP threshold (mV)	−36.3 ± .6	−33.4 ± .9	−35.7 ± 1.1	−36.6 ± .5
AP amplitude (mV)	105.3 ± 1.6	103.4 ± 1.2	99.3 ± 2.8	76.9 ± .8
AHP amplitude (mV)[a]	8.4 ± .6	14.5 ± 1.2	10.4 ± 2.1	32.9 ± .8
Spike half width (ms)	.90 ± .01	1.05 ± .05	.82 ± .03	.51 ± .02
Frequency first AP (Hz)[b]	14.9 ± .7	9.0 ± .8	68 ± 19	57.4 ± 3.6
Frequency last AP (Hz)	7.9 ± .4	8.7 ± .9	10.4 ± 1.6	33.8 ± 2.6

All values are mean ± *SEM*. All values are measured at the current step above threshold.
[a]AHP amplitude is measured from threshold to maximal afterhyperpolarization.
[b]Frequency is determined as the inverse of the first interspike interval or last interspikeinterval.
Abbreviations: RS = regular spiking; LS = late spiking; BF = burst firing; PV = parvalbumin; RMP = resting membrane potential; AP = action potential; AHP = afterhyperpolarization.

were examined by an 800–1,000 ms current injection with an amplitude evoking hyperpolarizations or depolarizations from −100 to −30 mV, in steps of 5–10 mV. We characterized three principal neuron types in the deep layers throughout the rostro-caudal extent of the PER and LEC network (Figure 1, Table 1 and Supporting Information Figure 1a–c), analyzing the following characteristics: (1) the presence of a voltage sag on hyperpolarization, (2) latency to the first spike, (3) burst firing (consistent frequency of Spikes 1 and 2), and (4) spike frequency adaptation (Beggs, Moyer, McGann, & Brown, 2000; Canto & Witter, 2012; Faulkner & Brown, 1999; Fuchs et al., 2016). Regular spiking (RS) neurons (58/81) showed a regular, adapting firing pattern and a hyperpolarization-induced voltage sag (2.4 ± .2 mV, Figure 1a, Table 1). Late spiking (LS) neurons (11/81) showed delayed firing (142.9 ± 13.3 ms) and lacked a voltage sag on hyperpolarization (Figure 1b, Table 1). Burst firing (BF) neurons (12/81) showed a voltage sag (2.5 ± .4 mV; Figure 1c, Table 1) on hyperpolarization and typically fired the first two action potentials at a high frequency (68.4 ± 19.0 Hz) after which action potential firing showed adaptation (Figure 1c).

3.2 | Stimulus-evoked synaptic input rarely evokes action potential firing in per and LEC deep layer principal neurons

The recruitment of the PER and LEC deep layers in response to an AiP synaptic stimulation was investigated by applying an electrical stimulus in the AiP superficial layers at the intensity evoking the maximal synaptic response in 74 principal neurons (average stimulus intensity was 754 ± 30 μA) while the voltage was clamped at −70 mV (Figure 2a,b). The stimulus was applied three times, with an interstimulus interval of 4 s; consecutively recorded responses were averaged. The majority of principal neurons (66/74, 89%) received synaptic input from the AiP superficial layers after electrical stimulation. The onset latency and peak amplitude of the synaptic response were compared between the three types of principal neurons. Although BF neurons were more prominently localized in the PER, RS, LS, and BF neurons did not differ in latency, in case the latency was corrected for the distance from the stimulus electrode (latency: $F(2,63) = 3.10$, $p = .052$). The peak synaptic response was also comparable between the three principal neuron subtypes ($F(2, 63) = .92$, $p = .4$; Figures 1e and 2b′,b″). The principal neurons are therefore combined into one experimental group and analyzed together ($n = 66$). Analysis of the evoked synaptic current revealed that the latency increased with distance along the rostro-caudal PER-LEC axis. If we assume a synaptic delay of .5 ms in all PER-LEC neurons, the propagation velocity of activity is described by the slope of the robust linear fit of the relationship between the latency of responses and distance to the stimulus electrode. AiP stimulation evoked activity which propagated with .199 m/s (Figure 2b′). The peak of responses was not related to the distance from the electrode (regression analysis n.s.; Figure 2b″) and had an average amplitude of 327 ± 38 pA.

To address the output of deep layer principal neurons in response to their synaptic input, the evoked postsynaptic potentials were recorded in current clamp (Figure 2c). Only 3 out of 51 principal neurons (1 BF and 2 RS neurons) fired a single action potential in response to synaptic input. The peak amplitude of the evoked postsynaptic potentials in non-firing principal neurons did not relate to distance from the stimulus electrode (regression analysis n.s.; Figure 2c′). Since stimulus application was repeated three times, we were able to address the success rate for the AiP evoked action potentials. The AiP stimulus evoked 3/3 times an action potential in 2 principal neurons and 1/3 times an action potential in 1 principal neuron (Figure 5h, black dots). This led to the probability of the AiP stimulus evoking an action potential in spiking neurons of .78 ± .07.

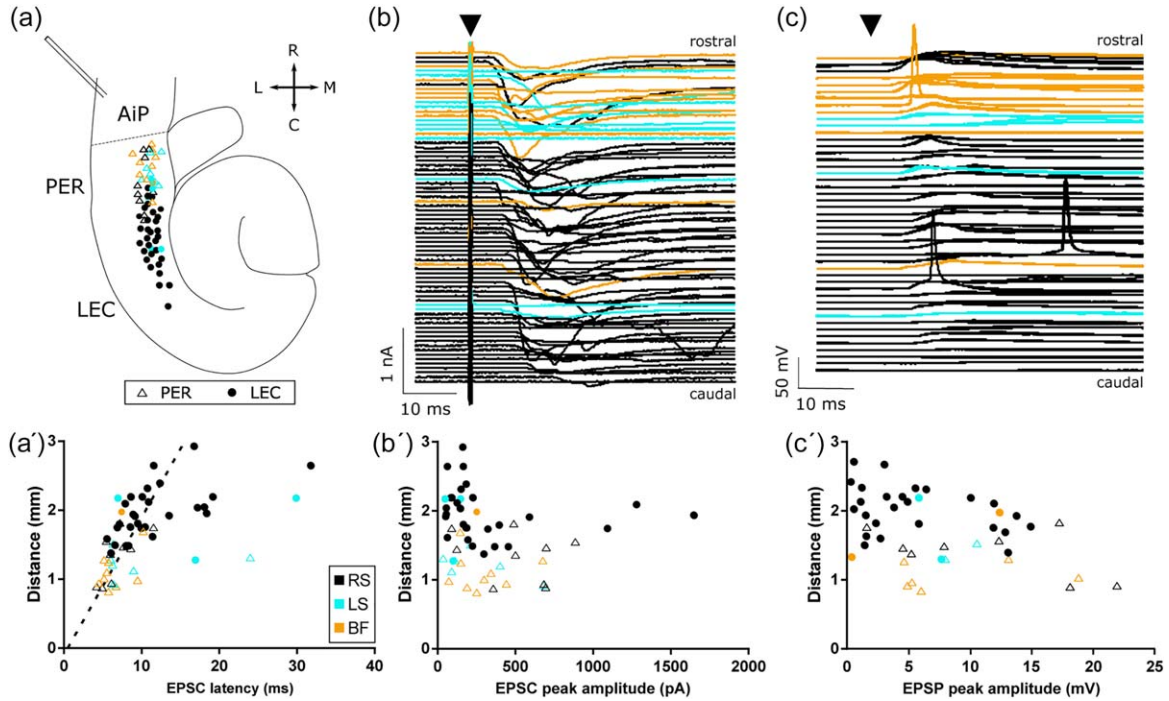

FIGURE 2 Evoked synaptic input and postsynaptic potentials in PER-LEC deep layer principal neurons. (a) Schematic overview of all principal neurons recorded in a horizontal mouse brain slice of one hemisphere containing the AiP (neocortical area), the PER and LEC. The stimulus electrode was placed in the AiP superficial layers. PER recorded cells are indicated with an open triangle (△) and LEC recorded cells are indicated with a closed circle (●). Colors represent three subtypes of principal neurons, that is, regular spiking (black), late spiking (cyan) and burst firing (orange) neurons. (b) AiP stimulus evoked postsynaptic currents in principal neurons sorted based on their distance to the stimulus electrode (colors represent three subtypes of principal neurons, see a). Principal neurons were voltage clamped at −70 mV, the arrowhead (▼) indicates the moment the stimulus was applied. (b′) The EPSC onset latency increased when recordings were performed at increasing distance from the AiP stimulus electrode ($n = 66$). Colors represent the three principal neuron subtypes. (b″) The stimulus electrode distance did not correlate with the EPSC peak amplitude. (c) Current clamp recordings of stimulus evoked postsynaptic potentials in 51 principal neurons. EPSPs were consecutively recorded three times at resting membrane potential. Only three out of 51 principal neurons responded with a single action potential after the stimulus, the other 48 neurons only showed an EPSP. Colors represent the three principal neuron subtypes. (c′) EPSP amplitude of the neurons which only showed an EPSP, so no firing, after stimulus application revealed no relationship between EPSP amplitude and the distance of the recorded neuron to the NC stimulus electrode. Colors represent the three principal neuron subtypes. Abbreviations: AiP, agranular insular cortex; PER, perirhinal cortex; LEC, lateral entorhinal cortex; R, rostral; C, caudal; L, lateral; M, medial; EPSC, excitatory postsynaptic current; RS, regular spiking; LS, late spiking; BF, burst firing; EPSP, excitatory postsynaptic potential; PrN, principal neuron. [Color figure can be viewed at wileyonlinelibrary.com]

3.3 | Synaptic input onto deep layer principal neurons is composed of a small excitatory and a larger inhibitory conductance

Since the deep layer principal neurons rarely emitted action potentials in response to a synaptic input, we hypothesized that the inhibition-excitation balance was in favor of inhibition and aimed to address the relation between the stimulus-evoked inhibition and excitation. The synaptic currents recorded at 4–5 holding potentials ranging from −90 to −50 mV in response to 50% and 100% of the maximum stimulus intensity (Figure 3b,c, insets) were used to estimate the synaptic conductance changes (Figure 3b,c) evoked by the afferent input in 53 principal neurons along the PER-LEC axis (Figure 3a). The evoked synaptic conductance at two stimulus intensities was linearly decomposed into an excitatory and inhibitory conductance during 100 ms, under the assumption of a reversal potential of 0 mV for excitation and −70 mV for the fast, chloride mediated $GABA_A$ dependent inhibition.

The latency of the evoked conductances was defined (Figure 3d). If an evoked conductance was detected ($n = 49$ principal neurons), the peak amplitude and half width were determined (Figure 3e,f). Combined evaluation of the latency, peak amplitude, and half width of the inhibitory and excitatory conductance revealed different dynamics for the evoked inhibitory and excitatory conductances after stimulation at the intensity evoking the maximum response (100% intensity) ($F(2.289, 110.3) = 22.68$, $p < .0001$). Sidak's multiple comparison post hoc analysis showed that the evoked excitatory conductance had a shorter latency than the evoked inhibitory conductance ($latency_{exc} = 7.2 \pm .4$ ms, $latency_{inh} = 10.5 \pm .6$ ms, $p < .0001$; Figure 3b–d), the peak of the inhibitory conductance was larger ($peak_{exc} = 3.8 \pm .5$ nS, $peak_{inh} = 8.4 \pm 1.1$ nS, $p < .0001$; Figure 3b,c,e), and the inhibitory response lasted longer (half $width_{exc} = 14.0 \pm 1.2$ ms, half $width_{inh} = 17.6 \pm 2.0$ ms, $p = .013$; Figure 3b,c,f) compared to the excitatory response. To examine whether the composition of synaptic responses changed when the input is weaker, we also stimulated the

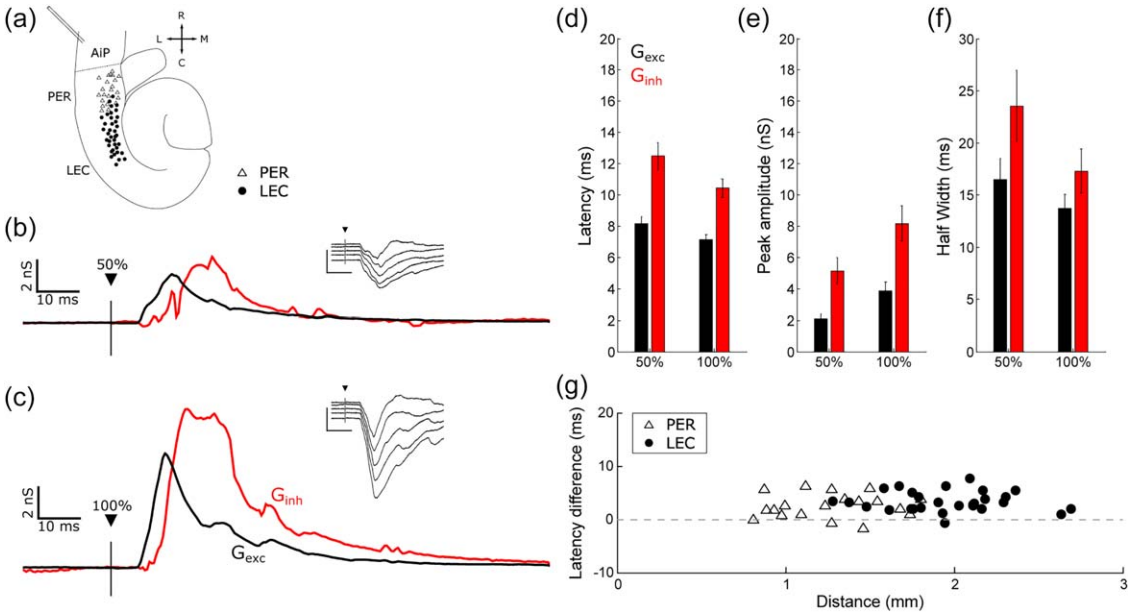

FIGURE 3 Evoked excitatory and inhibitory conductance in response to AiP stimulation at two intensities. (a) A schematic overview of the recorded PER (△) and LEC (●) principal neurons ($n = 48$). (b) Typical example of the G_{exc} (black trace) and the $GABA_A$ mediated G_{inh} (red trace) calculated from the evoked postsynaptic currents shown in the inset, evoked at 50% of the stimulus intensity evoking the maximum response. The arrowhead (▼) indicates the moment the stimulus is applied. (c) The G_{exc} (black trace) and the $GABA_A$ mediated G_{inh} (red trace) calculated from the evoked postsynaptic currents shown in the inset, of the same cell as in b but with 100% stimulus intensity. (d–f) Quantification of the onset latency (d), peak amplitude (e), and half width (f) of the G_{exc} (black) and G_{inh} (red) recorded in PER and LEC principal neurons at 50% and 100% of the stimulus intensity evoking the maximum response. (g) Plot of the difference between the G_{exc} and G_{inh} latency in relation to the distance from the stimulus electrode in the recorded PER and LEC principal neurons after stimulation at 100% intensity. Abbreviations: G_{exc}, excitatory conductance; G_{inh}, inhibitory conductance; PER, perirhinal cortex; LEC, entorhinal cortex; R, rostral; C, caudal; L, lateral; M, medial. [Color figure can be viewed at wileyonlinelibrary.com]

AiP at the intensity evoking the half maximum response (50% intensity, Figure 3b–f). We found that both excitation and inhibition had a slightly longer latency ($latency_{exc} = 8.2 \pm .4$ ms $p < .0001$, $latency_{inh} = 12.5 \pm .9$ ms, $p < .001$), lower peak amplitude ($peak_{exc} = 2.1 \pm .3$ nS $p < .001$, $peak_{inh} = 5.2 \pm .9$ nS $p < .0001$), and a comparable half width (half $width_{exc} = 16.5 \pm 2.0$ ms, half $width_{inh} = 23.5 \pm 3.4$ ms) compared to responses evoked at maximum stimulus intensity.

To address whether the delay between the recruitment of excitation and inhibition was different along the rostro-caudal axis of the PER and LEC, we tested whether the difference between the latency of the G_{exc} and G_{inh} changed with the distance from the stimulus electrode (Figure 3g). We found that there was no relation between the latency difference of the G_{exc} and G_{inh} and the distance (average delay was $3.3 \pm .4$ ms; regression analysis n.s., Figure 3g), indicating that the delay between excitation and inhibition does not depend on conduction velocity from the stimulus to the site of recording, which led to the hypothesis that G_{inh} is likely recruited in the local PER and LEC network.

3.4 | AiP evoked fast inhibition is recruited in the local per-LEC network

The latency of the inhibitory conductance we recorded in principal neurons was relatively short, which could imply the presence of direct, monosynaptic inhibitory input from the stimulated neocortical AiP. This hypothesis is in line with the long-range inhibitory projections from neocortical areas toward the PER and EC described by Pinto et al. (2006). To address the monosynaptic inhibition hypothesis, we bath applied ACSF containing 20 μM CNQX and 10 μM APV to block the AMPA and NMDA receptor mediated excitatory input. Besides mono and polysynaptic excitation, this prevents polysynaptic recruitment of interneurons in the local circuitry, only allowing possible monosynaptic, long-range GABAergic projections from the AiP to evoke an inhibitory response in principal neurons. After obtaining the AiP evoked conductances in control ACSF (Figure 4a), we obtained the conductances while excitatory transmission was blocked (Figure 4b). This abolished both excitatory and inhibitory conductances (Figure 4b,c, $p = .0018$, $n = 8$, Friedman test), suggesting the absence of a direct inhibitory connection from the AiP onto deep layer principal neurons in this mouse brain slice preparation. This implies that the inhibitory conductance evoked in PER-LEC deep layers must originate from local inhibitory neurons.

3.5 | PV interneurons are strongly recruited by synaptic input

AiP synaptic input to principal neurons in the PER-LEC network evoked a large inhibitory and a smaller excitatory synaptic conductance (Figure 3). PV expressing fast spiking interneurons are, amongst other

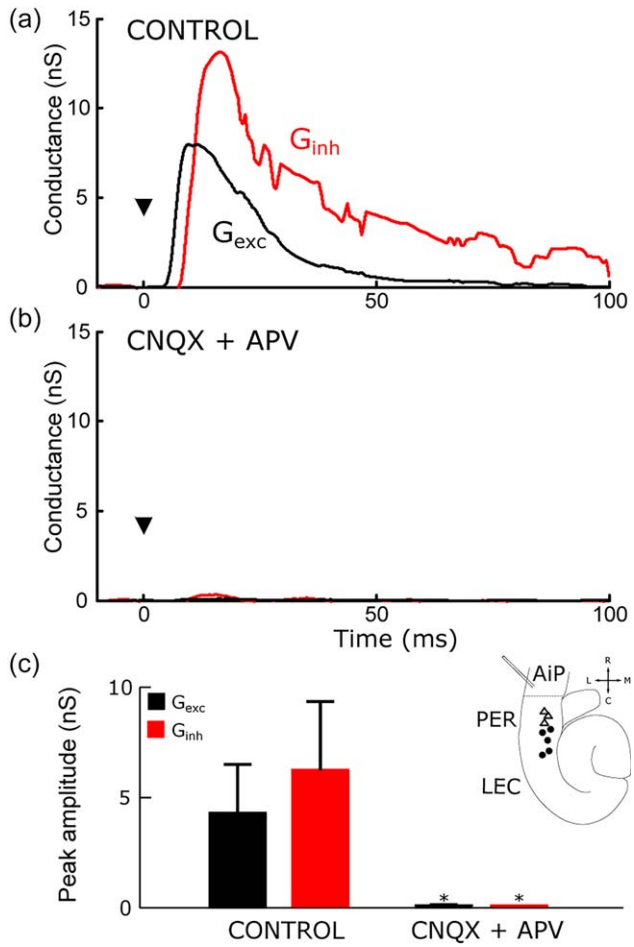

FIGURE 4 Both G_{exc} and G_{inh} disappeared after blocking the excitatory transmission with CNQX and APV. (a,b) Example of the G_{exc} (black trace) and G_{inh} (red trace) in an LEC neuron before (a) and after (b) the application of glutamate receptor blockers CNQX and APV. The arrowhead (▼)indicates the moment the stimulus is applied. (c) Quantification of the average evoked G_{exc} (black) and G_{inh} (red) before and after application of CNQX and APV ($n = 8$, * indicates $p < .05$). Inset shows the distribution of recorded principal neurons in the PER (△) and LEC (●). Abbreviations: AiP, agranular insular cortex; PER, perirhinal cortex; LEC, lateral entorhinal cortex; R, rostral; C, caudal; L, lateral; M, medial; G_{exc}, excitatory conductance; G_{inh}, inhibitory conductance. CNQX, 6-cyano-7-nitroquinoxaline-2,3-dione; APV, 2-amino-5-phosphonopentanoic acid. [Color figure can be viewed at wileyonlinelibrary.com]

interneuron types, present in the local PER and LEC network (Barinka et al., 2012; Wouterlood et al., 1995) and make synaptic contacts onto the axosomatic region of principal neurons (Klausberger & Somogyi, 2008; Kubota, Karube, Nomura, & Kawaguchi, 2016; Markram et al., 2004). PV interneurons are capable of high frequency firing on depolarization (Figure 1d), and can, therefore, exhibit strong inhibitory action onto principal neurons (Pfeffer et al., 2013). This led to the hypothesis that PV interneurons could well be strongly recruited by the AiP input, to account for the large, locally activated, inhibitory conductance (Figures 3 and 4). To address this hypothesis, the synaptic input (Figure 5a–d) and action potential firing (Figure 5e–h) in response to neocortical AiP stimulation was examined in horizontal slices of transgenic mice conditionally expressing YFP in PV interneurons (Supporting Information Figure 1d). PV interneurons were recorded along the rostro-caudal axis of the PER and LEC deep layer network (Figure 5a, left) and were characterized by a small membrane time constant, a lack of a hyperpolarization induced voltage sag, a short onset latency to the first induced action potential, and a smaller AP amplitude than principal neurons (Figure 1d,e, Table 1).

AiP stimulation evoked complex synaptic responses in 53/56 the PV interneurons (95%). Assuming a synaptic delay of .5 ms, the latency increased with distance from the stimulus electrode (slope = .192 mm/ms; Figure 5a right, b) and the peak amplitude of the response decreased with distance along the rostro-caudal extent of the PER and LEC (slope = −.0002 mm/pA, $R^2 = .32$, $F(1,51) = 24.01$, $p < .0001$; Figure 5a right, c). Long latencies were accompanied with a small peak amplitude (Figure 5d), at larger peak amplitudes, the latency did not show large values.

We next examined whether the PV interneurons fired action potentials in response to AiP stimulation (Figure 5e–h). We recorded 51 PV interneurons in current clamp to determine the postsynaptic potentials and evoked firing in response to AiP stimulation in three consecutive repeats. We found that in total 31/51 deep layer PV interneurons recorded over the whole extent of the PER and LEC (Figure 5a,e,f), fired action potentials in response to AiP stimuli with a success rate for the AiP evoked synaptic input of .90 ± .04 in firing PV interneurons. Assuming a constant synaptic delay of .5 ms, the latency of the first evoked spike increased with distance from the stimulus electrode (Figure 5h, slope = .158 mm/ms), with a velocity which was in the range of axonal conduction velocity (Telfeian & Connors, 2003; Willems et al., 2016). This conduction velocity was slightly lower than the velocity calculated based on the response latency, likely because of the combination of monosynaptic and polysynaptic origin of the responses, leading to more variable spike timing.

The standard deviation of the latency of the first evoked spike in all three consecutive repetitions in response to AiP stimulation was used as an indicator for the spike jitter and was 1.0 ± .6 ms, suggesting a very reproducible recruitment of PV interneurons directly after synaptic input is received. Although the peak of the evoked response decreased with distance along the PER-LEC rostro-caudal axis, the average frequency of the evoked firing in PV interneurons was not related to distance (regression analysis n.s.; Figure 5f). A subset of PV interneurons (4/31) persistently continued firing after the stimulus (Figure 5g,h) indicating that PV interneurons are strongly recruited in the PER and LEC network and can therefore exhibit strong inhibitory control onto deep layer principal neuron activity.

3.6 | Connectivity between local PV interneurons and principal neurons

Since local PV interneurons strongly respond to AiP synaptic input (Figure 5), we hypothesized that these PV interneurons project onto principal neurons locally in the PER-LEC deep layer network. To address the connectivity of deep layer PV interneurons and principal neurons in the PER and LEC deep layers, we performed 29 paired recordings of

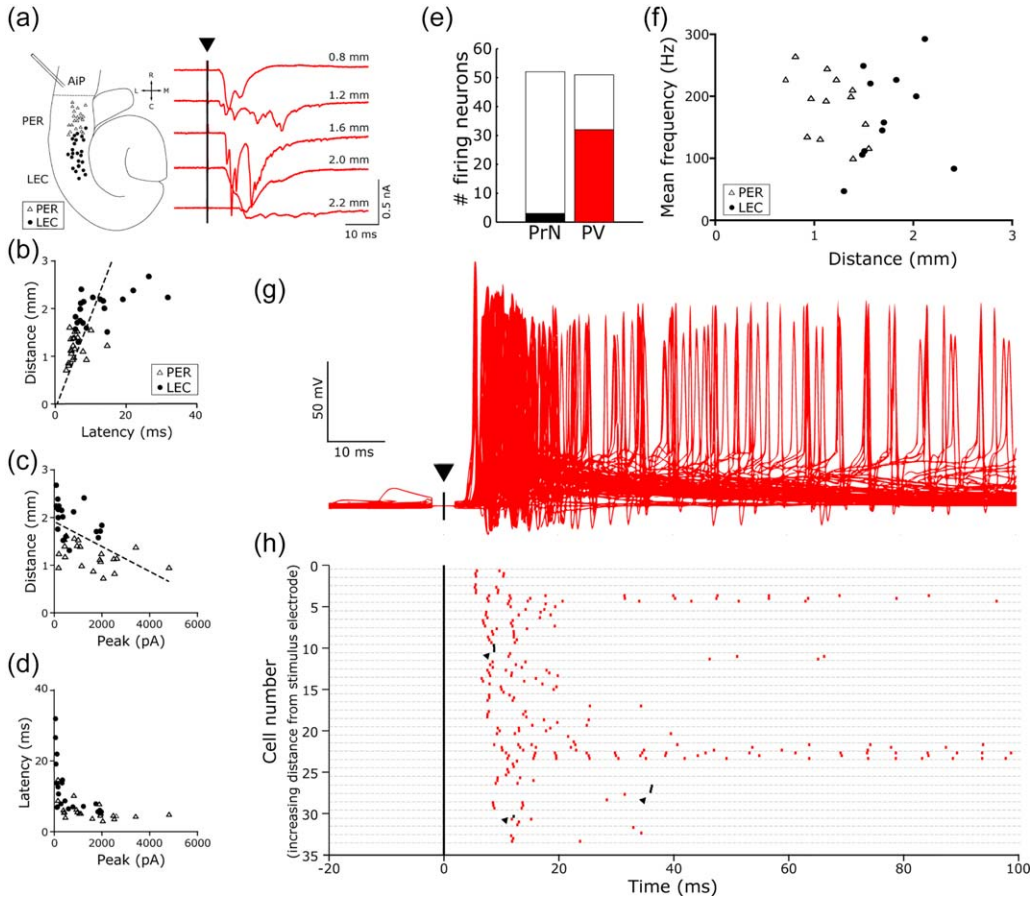

FIGURE 5 Recruitment of principal neurons and PV interneurons by AiP stimulation. (a) Left: Schematic overview of the distribution of recorded PV interneurons along the rostro-caudal extent of the PER (△) and LEC (●). Right: Five example traces of NC stimulus evoked synaptic input in deep layer PV interneurons, top to bottom traces represent recordings at increasing distances from the stimulus electrode. (b, c) Distance—onset latency (b) and distance—peak amplitude (c) relationship of PV synaptic evoked responses. (d) Relationship between the onset latency and peak amplitude of the evoked postsynaptic responses. (e) The portion of principal neurons (black) and PV interneurons (red) of the recorded population which responded to the stimulus with action potential firing. (f) Relationship between the stimulus-evoked firing frequency in PV interneurons and the distance from the recorded neuron to the stimulus electrode. (g) The stimulus evoked action potential firing of PV interneurons. (h) The spike raster plot showing the evoked firing of principal neurons (black dots, indicated with the arrowhead) and PV interneurons (red dots). The neurons are sorted on the *y*-axis from closest to farthest from the stimulus electrode. Abbreviations: AiP, agranular insular cortex; PER, perirhinal cortex; LEC, lateral entorhinal cortex; R, rostral; C, caudal; L, lateral; M, medial; PrN, principal neuron; PV, parvalbumin interneuron. [Color figure can be viewed at wileyonlinelibrary.com]

principal neurons and PV interneurons. After successfully obtaining whole-cell configuration in both neurons within a 200 μm interneuron-distance, random frozen noise was injected in the principal neuron or PV interneuron to evoke reproducible, randomly distributed action potential firing at an average frequency of 1–2 Hz (Figure 6a,b). Principal neuron-PV pairs were considered connected when the onset of the unitary postsynaptic currents (uEPSC or uIPSC) following the evoked spikes clustered within 4 ms after the spikes (Figure 6a″,b″) and the probability of spike transmission was at least .6 (Csicsvari, Hirase, Czurko, & Buzsáki, 1998; Miles, 1990).

First, principal neuron firing was induced and the PV interneuron was clamped at −70 mV to simultaneously record uEPSCs in response to a principal neuron action potential (Figure 6a,a′). In 11/29 recordings (38%), the principal neuron projected onto the simultaneously recorded PV interneuron (Figure 6a,a″). The latency of the uEPSC in the PV neuron was 2.5 ± .2 ms after the peak of the principal neuron action potential (Figure 6c, $n = 312$ action potentials from 11 principal neurons). The uEPSC rise time in PV interneurons was .61 ± .15 ms (Figure 6d). The probability of the principal neuron spike evoking a uEPSC was .83 ± .04 in the 11 connected principal neuron to PV interneuron pairs (Figure 6e).

Second, the projection from a PV interneuron onto a principal neuron was tested by recording PV interneuron firing-induced uIPSCs in the principal neuron, clamped at −50 mV to reveal the outward inhibitory currents (Figure 6b,b′). In 14% of the pairs (4/29), a PV to principal neuron projection was detected. The latency of the uIPSCs was 1.33 ± .05 ms after peak time of the PV spike (Figure 6b″,c, $n = 99$ action potentials from 4 PV interneurons). The uIPSC rise time in principal neurons was 2.68 ± .15 ms (Figure 6d). The probability that a PV spike evoked a uIPSC was high, .98 ± .025 (Figure 6e, $n = 4$ pairs). Although the latencies of both uEPSCs and uIPSCs showed a comparable

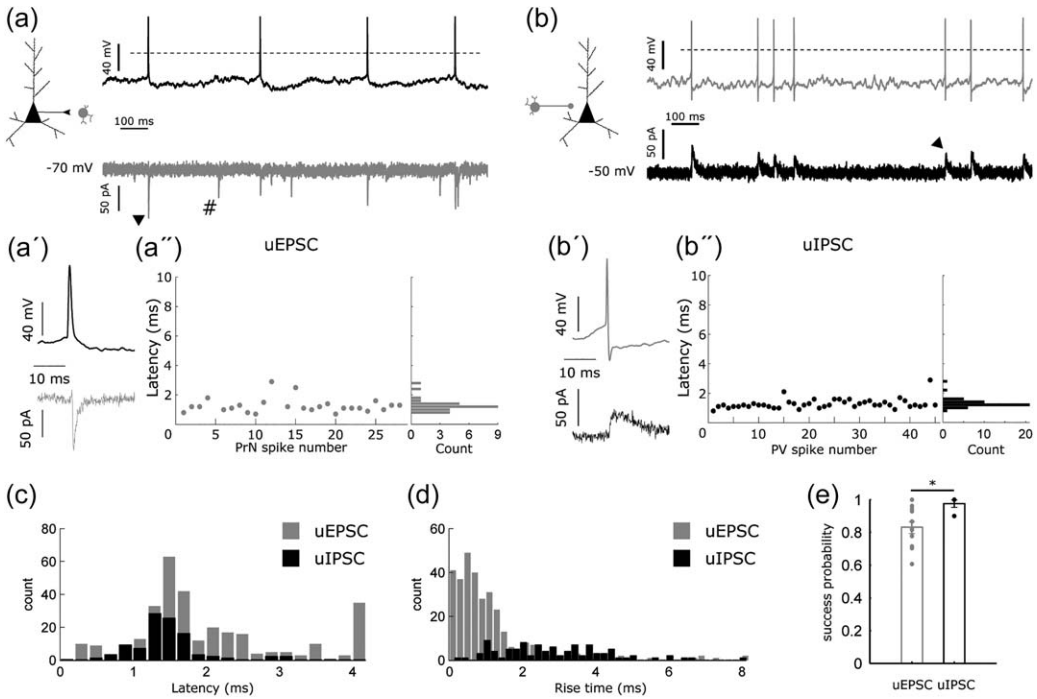

FIGURE 6 Connectivity between principal neurons and PV interneurons in the deep layers of the PER-LEC network. (a,a″) Typical example of a principal neuron to PV interneuron monosynaptic projection. (a) Left: Schematic overview of the stimulated principal neuron (black) and recorded PV interneuron (gray). Top trace (black) shows the evoked firing in response to current injection in the principal neuron (dashed line indicates 0 mV) and the bottom trace (gray) shows the recorded excitatory currents at −70 mV holding potential, both spontaneous (example indicated with #) and spike evoked (example indicated with ▼). (a′) Magnification of the evoked action potential in the principal neuron (top, black trace) and the corresponding spike evoked unitary EPSC (uEPSC, bottom, gray trace), indicated with a ▼ in a′, in the PV interneuron. (a″) The uEPSC latency was consistent in the PV interneuron after a spike in the principal neuron and a narrow distribution of uEPSC latencies was found after principal neuron firing. (b,b″) Typical example of a PV interneuron to principal neuron connection. (b) Left: Schematic overview of the stimulated PV interneuron (gray) and the principal neuron (black) recorded at a −50 mV holding potential. Top trace (gray) shows the action potential firing evoked in the PV interneuron (dashed line indicates 0 mV), bottom traces (black) represents the recording in the principal neuron. Inhibitory currents are outward and excitatory currents are inward at this holding potential. (b′) Magnification of the PV interneuron action potential (top) and the corresponding outward inhibitory current (bottom) in the principal neuron of the spike evoked current indicated with a ▼ in b. (b″) The uIPSC latency was consistent after a spike in the PV interneuron and a narrow distribution of uIPSC latencies was found after PV interneuron firing. (c) Frequency distribution of the latencies (bin = .2 ms) of the uEPSCs (gray) and uIPSCs (black) pooled for all evoked action potentials ($n = 312$ uEPSCs from 11 pairs and $n = 99$ uIPSCs from 4 pairs). (d) Frequency distribution of the rise time (bin = .2 ms) of uEPSCs (gray) and uIPSCs (black). (e) The success probability of a spike evoking a uEPSC (gray) and uIPSC (black) in the connected pairs, showing a larger success rate for PV interneuron spikes evoking a uIPSC than principal neurons evoking a uEPSC (* indicates $p < .05$). Abbreviations: IPSC, inhibitory postsynaptic current; EPSC, excitatory postsynaptic current

distribution (Figure 6c), the distribution of the rise time of uEPSCs was skewed compared to the distribution of the rise time of uIPSCs (Figure 6d), indicating that uEPSCs had faster kinetics than uIPSCs.

Only a subset (45%) of the recorded pairs was connected, 52% of the recorded pairs were not connected in this study and 2/29 recorded pairs (7%) were reciprocally connected.

3.7 | Relation between synaptically evoked PV firing and inhibitory conductance in principal neurons

We next examined if PV interneurons could induce the fast, large inhibitory conductance observed in principal neurons in the local deep layer PER and LEC network. The temporal dynamics of PV interneuron recruitment should be fast enough to explain the fast inhibitory conductance which we recorded in the principal neurons (Figure 3). To compare the recruitment of the PV and principal neurons in response to AiP stimulation, we simultaneously recorded evoked synaptic currents in principal neurons and PV interneurons ($n = 18$ pairs, Figure 7a). The latency of the evoked synaptic responses in the PV interneurons (8.5 ± .9 ms) was shorter than in principal neurons (10.7 ± 1.3 ms; $t(17) = 2.5$, $p = .02$; Figure 7b,c). The peak amplitude of the evoked synaptic response in PV interneurons (714 ± 165 pA) was larger than the evoked synaptic response in principal neurons (343 ± 104 pA; $t(17) = 3.1$, $p = .007$; Figure 7b,d). These results suggest, together with the absence of firing in principal neurons (Figures 2 and 6), that AiP stimulation recruits the inhibitory network predominantly in a feedforward manner. Furthermore, the conduction velocity of the synaptic input in both principal neurons and PV interneurons was comparable, suggesting that both types receive input from the same axon fibers.

Finally, we examined the relation between PV firing and the evoked inhibitory conductance in principal neurons in simultaneously

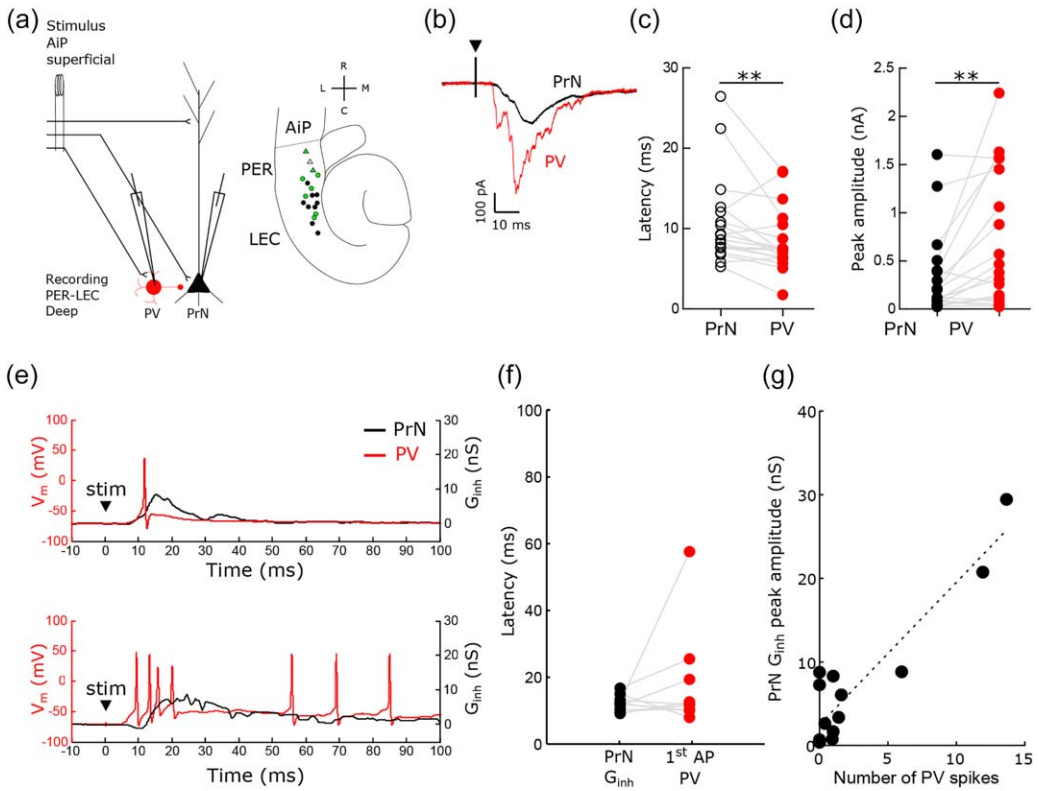

FIGURE 7 Input and output of PV interneurons and principal neurons recorded simultaneously along the PER-LEC axis. (a) Left: Schematic representation of the stimulation and recording configuration with the excitatory input from the AiP superficial layers in black, the deep layer principal neuron in black and the PV neuron in red. Right: schematic representation of the distribution of PER (△) and LEC (●) recorded pairs. Markers of coupled pairs are filled green, uncoupled pairs are shown with a white (PER) or black (LEC) fill. (b) Typical example of the evoked postsynaptic currents recorded in a principal neuron (black) - PV interneuron pair (red), both clamped at −70 mV. (c,d) Onset latency (c) and peak amplitude (d) of stimulus evoked responses in principal neuron (black) - PV interneuron (red) pairs ($n = 18$ pairs), connecting lines indicate the simultaneously recorded principal and PV neuron (** indicates $p < .01$). (e) 2 typical examples of simultaneously recorded stimulus evoked G_{inh} in the principal neuron (black trace) and action potential firing in the PV interneuron (red trace). The arrowhead (▼) represents the moment of stimulus application. (f) Comparison of the onset latency of stimulus evoked G_{inh} in the principal neuron (black) and the latency of the first PV spike (red) recorded simultaneously. (g) The relationship between the average number of PV spikes evoked after stimulus application and the peak amplitude of the simultaneously recorded G_{inh} in the principal neuron. Abbreviations: AiP, agranular insular cortex; PER, perirhinal cortex; LEC, lateral entorhinal cortex; R, rostral; C, caudal; L, lateral; M, medial; PV, parvalbumin positive interneuron; PrN, principal neuron; G_{inh}, inhibitory conductance. [Color figure can be viewed at wileyonlinelibrary.com]

recorded PV-principle neuron pairs. We compared the peak latency of the first PV spike to the G_{inh} onset latency in the simultaneously recorded principal neuron in response to an AiP stimulus (Figure 7e). We found that the latency of the G_{inh} and the latency of the first evoked PV spike were not different (Figure 7f; Wilcoxon signed rank test n.s., $n = 9$ pairs). Additionally, the number of emitted spikes in the PV neuron strongly correlated with the peak G_{inh} in the simultaneously recorded principal neuron (Figure 7g; $R^2 = .84$, $p < .0001$, $n = 14$ pairs), indicating that the number of spikes in the PV interneuron predicts the amount of inhibition in the simultaneously recorded principal neuron.

To get an indication of the necessary inhibitory input onto principal neurons in response to AiP stimulation, we estimated which inhibitory spike pattern was needed to reconstruct the recorded G_{inh} in principal neurons. The mean time locked uIPSC in the principal neuron that was linked to a single action potential from the PV interneuron (Figures 6 and 8a), allowed us to determine the conductance change of such single response, using the uIPSC and the driving force to calculate the unitary G_{inh} (uG_{inh}). Subsequently, all recorded uG_{inh} traces ($n = 101$ uG_{inh} from four connected PV-principal neuron pairs recorded in four mice) were averaged to obtain one standardized uG_{inh} (Figure 8a). Using this standard PV interneuron firing-induced uG_{inh}, we could reconstruct the hypothetical pattern of inhibitory input received by a principal cell based on the firing patterns we recorded from the PV neurons (Figure 5). As shown above, 31 out of 51 PV interneurons emitted action potentials in response to AiP stimulation (Figure 5e) and stimulation was repeated three times. Most, but not all, PV interneurons responded three out of three consecutive recorded repeats (Figure 5h), which resulted in 83 AiP-evoked PV spike patterns. Figure 8b (top traces) shows examples of six typical PV spike patterns. We assumed that the 83 recorded spike patterns describe a representative set of PV interneurons, which characteristically responded to the synaptic input.

Next, the predicted G_{inh} evoked by these 83 spike patterns were calculated using the standard uG_{inh} (examples are shown in Figure 8b, bottom traces). The 83 predicted G_{inh} traces were used to perform a nonnegative linear regression fit (Matlab) to find the weight of every PV interneuron spike pattern to reconstruct the recorded G_{inh} in a

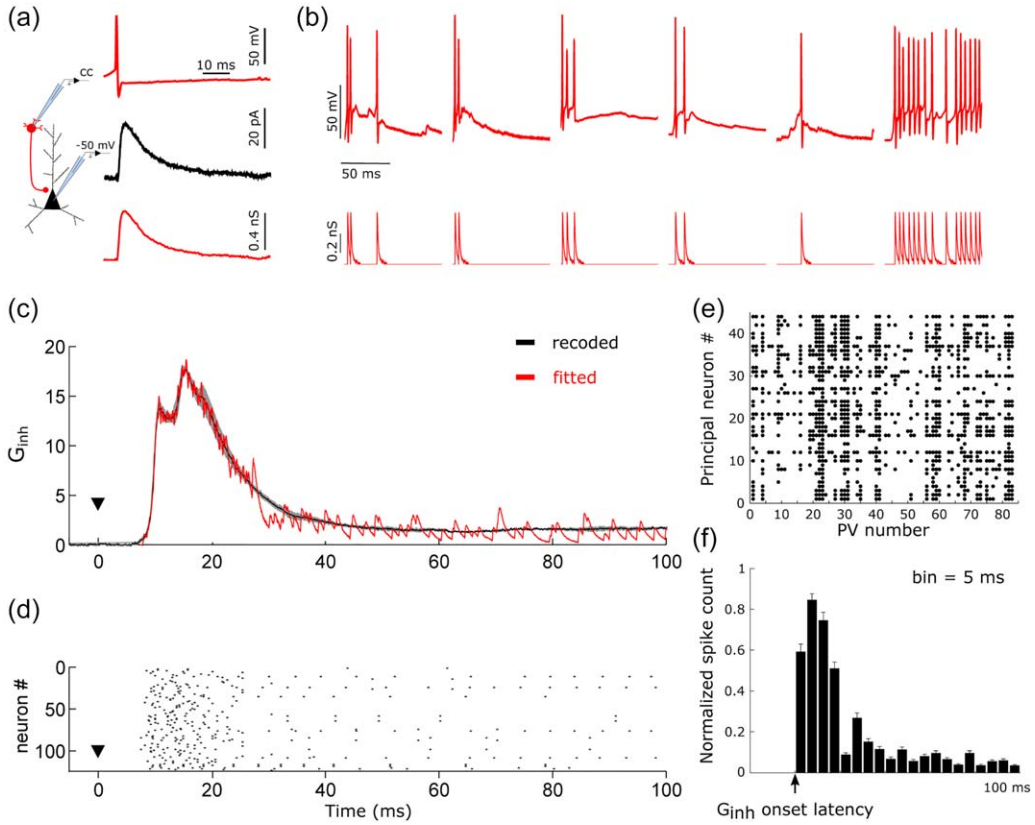

FIGURE 8 Prediction of inhibitory input received by principal neurons. (a) Recording of a principal neuron—PV interneuron pair (left shows schematic overview). Action potential in the PV interneuron (top, red trace) evoked a uIPSC in the principal neuron (middle, black trace, average of 101 uIPSCs, $n = 4$ animals) at −50 mV holding potential. The bottom trace shows the average calculated unitary G_{inh} the PV spikes evoked in a principal neuron (average of 101 uG_{inh}, $n = 4$ animals, shaded errorbar shows the *SEM*). (b) Top: example traces of AiP stimulation evoked spikes in six PV interneurons. Bottom: reconstructed inhibitory conductance that each PV spike pattern would have evoked in the postsynaptic principal neurons. (c) Typical example of the evoked G_{inh} in a principal neuron (black trace). The evoked G_{inh} was fit with the inhibitory conductance pattern of PV interneurons (red trace). The arrowhead (▼) represents the moment of stimulus application. (d) The weight of every spike pattern was used to assemble the reconstructed raster plot of inhibitory spikes the principal neuron shown in c received in time, randomly ordered. (e) Distribution of which spike patterns of interneurons were necessary for reconstruction of the G_{inh} in every principal neuron. (f) Poststimulus-time-histogram of the normalized spike distribution in 44 principal neurons of which the G_{inh} was reconstructed. The spike distribution of the principal neurons was averaged and then normalized to the bin with the maximum spike count. Arrow indicates the onset latency of the response in the principal neuron. Abbreviations: AiP, agranular insular cortex; uIPSC, unitary inhibitory postsynaptic current; G_{inh}, inhibitory conductance. [Color figure can be viewed at wileyonlinelibrary.com]

principal neuron. A constraint was that the weight of the predicted G_{inh} of every PV interneuron included, had to be at least 1. Figure 8c shows a typical example of a recorded (black trace) G_{inh} in a principal neuron and the accompanying predicted G_{inh} (red trace). In this typical example, 41 PV interneuron spike patterns, all with weights between 1 and 5, were required to reconstruct the recorded G_{inh} in this principal neuron. The number of PV interneuron spike patterns and their weights were used to reconstruct the inhibitory spike pattern the principal neurons would have received, by multiplying the 41 included PV spike patterns by their weights and in that way creating the predicted spike raster plot of the total inhibitory spike pattern (Figure 8d). We were able to fit the recorded G_{inh} of 49 principal neurons. Figure 8e shows which PV spike patterns were included for each principal neuron G_{inh} reconstruction. With the population of 83 PV spike patterns we had enough variation in inhibitory spike patterns to reconstruct the recorded G_{inh} in all 49 principal neurons.

To address when the majority of inhibitory spikes have to occur to evoke the recorded G_{inh}, we reconstructed peristimulus time histogram (PSTH). The PTSH was normalized to the onset latency of the recorded G_{inh}, binned, averaged over the PSTH of the 44 principal neurons of which the inhibitory spike pattern was reconstructed and normalized to the bin with the maximum spike count (Figure 8f). The inhibitory activity was most prominent in the first 20 ms of the inhibitory input, but continues during the time course of 100 ms with fewer spikes, probably to create long lasting suppression of activity within the PER-LEC network. We predicted that principal neurons received 4–733 inhibitory spikes in response to AiP stimulation, based on the 49 reconstructed spike patterns. In conclusion, with our set of recorded PV

interneurons, with differential stimulus evoked spike patterns, we could explain the G_{inh} recorded in all 49 principal neurons.

4 | DISCUSSION

Information from the neocortex travelling toward the hippocampus for memory consolidation is relayed by the PER-LEC network (Buzsáki, 1996; Pennartz, Uylings, Barnes, & McNaughton, 2002), where transmission is most likely regulated by inhibition (de Curtis & Paré, 2004). This study addressed the recruitment of the inhibitory and excitatory neuronal local circuitry in the deep layers of the PER and LEC network of the mouse. Stimulation of the superficial layers of the AiP, a neocortical afferent of the PER and LEC, revealed that the PV interneurons are involved in eliciting strong inhibition of principal neurons in the deep layer network.

4.1 | Three per-LEC principal neuron types and their evoked synaptic input

We recorded principal neurons in the deep layers of the PER-LEC network because the LEC deep layers are considered to play a significant role in gating activity transmission, likely regulated by the inhibitory circuitry (Koganezawa et al., 2008; Willems et al., 2016). Examination of the intrinsic properties like the hyperpolarization-induced sag and firing properties of these deep layer principal neurons revealed three subtypes, that is, RS, LS, and BF neurons in mouse brain slices, which are comparable with the assumed excitatory, glutamate containing neurons in rats (Faulkner & Brown, 1999; Moyer, McNay, & Brown, 2002; Somogyi, Tamás, Lujan, & Buhl, 1998) and guinea pigs (Martina et al., 2001).

Superficial AiP stimulation evoked synaptic responses in both PER and LEC deep layer principal neurons. The three subclasses responded similarly to AiP stimulation, as the latency and peak amplitude did not differ and all types refrained from action potential firing. This phenomenon might depend on the stimulated afferent, as seen in the piriform cortex, where BF and RS neurons respond similarly to layer Ib, but differentially to lateral olfactory tract input (Suzuki & Bekkers, 2006). Our data suggest that synaptic input from the AiP to PER-LEC deep layer neurons is not principal neuron subtype specific. It is, however, still possible that these neuronal subtypes react differently to the same synaptic input when the membrane potential is around firing threshold, as a result of their different intrinsic properties. Since the evoked EPSP almost never induced action potential firing in these experiments, the three subtypes of principal neurons were pooled.

The latency of the synaptic input in principal neurons gradually increased with the distance from the stimulation electrode, comparable with findings of Biella et al. (2001) and Unal, Apergis-Schoute, and Paré (2012). The synaptic input is shown to be both mono and polysynaptic in deep layer PER and LEC neurons (Burwell & Amaral, 1998a; Deacon, Eichenbaum, Rosenberg, & Eckmann, 1983; Unal et al., 2013; de Villers-Sidani, Tahvildari, & Alonso, 2004). A combination of conduction velocity, distance, and polysynaptically transmitted activity can explain the increasing latency of synaptic responses in neurons situated more caudal in the PER-LEC network. The polysynaptic response in the LEC could originate from PER neurons projecting to the apical dendrites of LEC deep layer neurons (Biella et al., 2002; Burwell & Amaral, 1998b; de Villers-Sidani et al., 2004). Both the peak EPSC and EPSP in principal neurons were not related to distance along the rostro-caudal axis, suggesting no difference between PER and LEC excitation. This finding is in line with Mathiasen et al. (2015) who did a tracing study showing that the neocortical AiP is a presynaptic target of both deep layer PER and deep layer LEC neurons in the rat.

4.2 | Output of principal neurons and PV interneurons

Although 89% of the recorded principal neurons received synaptic input, only 6% (3 out of 51) of them spiked, while 61% (31 out of 51) of the PV neurons fired after AiP stimulation in this horizontal mouse brain preparation. Pelletier et al. (2004) found percentages of firing neurons in the deep layers of the PER (40%) and the EC (1.4%) in vivo. These results together suggest that superficial layer AiP can evoke synaptic activity in deep layer PER and LEC principal neurons, but this activity is not transmitted from the LEC to the postsynaptic targets (Biella et al., 2002). However, since the brain consists of approximately 80% excitatory neurons and 20% inhibitory neurons (Markram et al., 2004), this small percentage of firing principal neurons might be effective. If we take an example population of 1,000 neurons, there will be 800 principal neurons and 200 interneurons. We found 6% firing principal neurons, resulting in 48 (800*.06) firing principal neurons, and 61% firing PV interneurons, leading to 122 PV interneurons firing action potentials in response to an input in our example population. This finding supports the sparse coding strategy, which assumes that only a small portion of the cortical principal neurons fire in a certain event, responsible for information transfer in the EC-hippocampal circuitry (Mizuseki & Buzsáki, 2013) and this balance might be critical to maintain a self-organized and controlled activity in large scale networks. Furthermore, computer models showed that a small portion of firing excitatory neurons with strong synaptic weights can be sufficient to have ongoing network activity (Ikegaya et al., 2013).

4.3 | AiP recruits feedforward inhibition

The low firing probability of principal neurons in response to synaptic input could be due to a marginal excitatory input or a massive inhibition. We found that AiP stimulation evoked a larger inhibitory than excitatory conductance in the PER-LEC deep layer principal neurons, suggesting more $GABA_A$ than glutamate receptor activation at principal neuron postsynapses. This phenomenon is not necessarily surprising since a larger inhibitory synaptic conductance than excitatory conductance can lead to balanced inhibitory and excitatory synaptic currents, due to a smaller driving force for inhibition than for excitation (Puzerey & Galán, 2014). However, the short latency difference between the excitatory and inhibitory conductance and especially the larger, longer lasting inhibitory conductance could prevent firing of deep layer principal neurons once they are depolarized.

It has been previously shown that stimulation of the temporal neocortex in brain slices of guinea pigs evoked a pure excitatory response when the recording electrode was more than 1 mm away from the stimulus electrode, while more closely situated neurons showed a sequence of excitatory and inhibitory potentials (Martina et al., 2001). In contrast, in this study we find both excitatory and inhibitory evoked components recruited in the same fashion along the rostro-caudal extent of the PER and LEC network. This indicates that the AiP projections in mouse horizontal brain slices evoke both excitation and inhibition in the whole PER-LEC network.

A broad range of interneurons are defined, based on several characteristics like morphology, physiological, and connectional properties. Good candidates for delivering strong inhibition on principal neurons are the PV expressing interneurons. These interneurons target the axosomatic region of neurons and therefore evoke large inhibitory currents in the postsynaptic neuron on firing (Jiang et al., 2015; Pfeffer et al., 2013). The PV neurons received a larger evoked synaptic current than principal neurons, which can be due to the presence of larger or more glutamatergic terminals on interneuron dendrites, resulting in more effective activity transmission in interneurons (for review see Buzsáki, Kaila, & Raichle, 2007). This fits neatly with the discovered PV firing patterns, often showing multiple action potentials, at a high frequency, in response to AiP stimulation. Although the role of different interneuron subtypes in evoking the large G_{inh} in principal neurons is not yet clear, we showed a complete reconstruction of the recorded G_{inh} in principal neurons solely based on the firing patterns of PV interneurons. This indicates that variation of responses in PV interneurons possibly is enough to explain the inhibitory input in principal neurons. Future studies may reveal the role of other interneuron types in this large G_{inh} in the PER-LEC deep layer principal neurons.

Moreover, the synaptic input from the AiP is first received by PV and then by principal neurons in the PER and LEC deep layers when simultaneously recorded and the principal did not fire in response to AiP stimulation. Based on the comparable conduction velocities derived from the evoked EPSCs in principal neurons and PV interneurons we surmise that the same fibers innervate both neuron types. We, therefore, propose that deep layer PV interneurons are recruited in a feedforward manner by the AiP synaptic input and substantially contribute to strong principal neuron inhibition in the PER and LEC network. This is supported by anatomical data showing a high incidence of excitatory projections from the PER to GABAergic neurons in the EC (Pinto et al., 2006). However, since bidirectional connections between PV and principal neurons are found, it is still likely that PV neurons can also provide feedback inhibition if local principal neuron would fire.

4.4 | Functional relevance of feedforward inhibition in the per-LEC network

The recruitment of feedforward inhibition preventing deep layer principal neurons from firing can have two plausible functions: First, inhibition of activity in the deep layers in response to superficial neocortical input is in line with the general hypothesis that information travelling toward the hippocampus is mainly transmitted via the superficial layers of the PER-EC network (Ruth, Collier, & Routtenberg, 1988; Witter, 1993) and that the deep layers return the information from the hippocampus to the neocortical areas (Buzsáki, 1996; Canto, Wouterlood, & Witter, 2008). We, therefore, hypothesize that this strong inhibitory response in the deep layers blocks the output pathway of the hippocampus, while possibly facilitating the input pathway via the superficial layers. This hypothesis is supported by data showing that PER superficial layer stimulation results in a significant monosynaptic activation of LEC superficial dendrites (de Villers-Sidani et al., 2004). Besides, a current source is found in layer V of the LEC in vivo, which could either be the result of apical dendrite activation of layer V principal neurons or deep layer inhibition (de Villers-Sidani et al., 2004). A similar concept of blocking activity propagation was found for regulation of the output from the hippocampus toward the EC (Gnatkovsky & de Curtis, 2006). They showed that the hippocampal output transfers through the EC deep layers, while the superficial MEC neurons were simultaneously inhibited, leaving only MEC deep layer neurons excitable by synaptic input arriving from the hippocampus.

Second, PV interneuron activity can be controlled by inputs from regulatory regions. By inhibiting the interneuron mediated inhibition, a window of opportunity could be created to transmit activity through the PER and EC. For example, cholinergic inputs from the basal forebrain regulate inhibitory activity in the EC as well as in the auditory cortex (Apergis-Schoute, Pinto, & Paré, 2007; Kuchibhotla et al., 2016) and hippocampal long range inhibitory projections to the EC specifically target interneurons (Melzer et al., 2012). Such mechanism would be useful to release the EC from a strong intrinsic inhibitory control, to regulate information transmission to the hippocampus.

Altogether, our study shows a strong recruitment of PV interneuron mediated inhibition in the deep layers of the PER and LEC network by the neocortical AiP. This inhibition is likely to play a key role in regulating selective transmission of information travelling to and coming from the hippocampus.

ACKNOWLEDGMENTS

We gratefully thank Lieneke Kooijman for the help with the immunohistochemistry, Hendrikus van Heesbeen and Christiaan Levelt for providing the eYFP-floxed and PV-Cre animals, respectively, and the Van Leeuwenhoek Centre for Advanced Microscopy for help with the confocal imaging.

CONFLICT OF INTEREST

The authors declare no competing financial interests.

ORCID

Janske G. P. Willems http://orcid.org/0000-0001-9516-7329

REFERENCES

Apergis-Schoute, J., Pinto, A., & Paré, D. (2007). Muscarinic control of long-range GABAergic inhibition within the rhinal cortices. *Journal of Neuroscience*, *27*, 4061–4071.

Assaf, F., & Schiller, Y. (2016). The antiepileptic and ictogenic effects of optogenetic neurostimulation of PV-expressing interneurons. *Journal of Neurophysiology*, *116*, 1694–1704.

Barinka, F., Salaj, M., Rybář, J., Krajčovičová, E., Kubová, H., & Druga, R. (2012). Calretinin, parvalbumin and calbindin immunoreactive interneurons in perirhinal cortex and temporal area Te3V of the rat brain: Qualitative and quantitative analyses. *Brain Research*, *1436*, 68–80.

Beggs, J. M., Moyer, J. R., McGann, J. P., & Brown, T. H. (2000). Prolonged synaptic integration in perirhinal cortical neurons. *Journal of Neurophysiology*, *83*, 3294–3298.

Biagini, G., D'antuono, M., Benini, R., de Guzman, P., Longo, D., & Avoli, M. (2013). Perirhinal cortex and temporal lobe epilepsy. *Frontiers in Cellular Neuroscience*, *7*, 130.

Biella, G., Uva, L., & Curtis, M. D. (2001). Network activity evoked by neocortical stimulation in area 36 of the guinea pig perirhinal cortex. *Journal of Neurophysiology*, *86*, 164–172.

Biella, G., Uva, L., & de Curtis, M. (2002). Propagation of neuronal activity along the neocortical-perirhinal-entorhinal pathway in the guinea pig. *Journal of Neuroscience*, *22*, 9972–9979.

von Bohlen und Halbach, O., & Albrecht, D. (2002). Reciprocal connections of the hippocampal area CA1, the lateral nucleus of the amygdala and cortical areas in a combined horizontal slice preparation. *Neuroscience Research*, *44*, 91–100.

Burwell, R. D. (2000). The parahippocampal region: Corticocortical connectivity. *Annals of the New York Academy of Sciences*, *911*, 25–42.

Burwell, R. D., & Amaral, D. G. (1998a). Cortical afferents of the perirhinal, postrhinal, and entorhinal cortices of the rat. *Journal of Comparative Neurology*, *398*, 179–205.

Burwell, R. D., & Amaral, D. G. (1998b). Perirhinal and postrhinal cortices of the rat: Interconnectivity and connections with the entorhinal cortex. *Journal of Comparative Neurology*, *391*, 293–321.

Buzsáki, G. (1996). The hippocampo-neocortical dialogue. *Cerebral Cortex*, *6*, 81–92.

Buzsáki, G., Kaila, K., & Raichle, M. (2007). Inhibition and brain work. *Neuron*, *56*, 771–783.

Canto, C. B., & Witter, M. P. (2012). Cellular properties of principal neurons in the rat entorhinal cortex. I. The lateral entorhinal cortex. *Hippocampus*, *22*, 1256–1276.

Canto, C. B., Wouterlood, F. G., & Witter, M. P. (2008). What does the anatomical organization of the entorhinal cortex tell us? *Neural Plasticity*, *2008*, 381243.

Csicsvari, J., Hirase, H., Czurko, A., & Buzsáki, G. (1998). Reliability and state dependence of pyramidal cell–interneuron synapses in the hippocampus: An ensemble approach in the behaving rat. *Neuron*, *21*, 179–189.

Cunningham, M. O., Hunt, J., Middleton, S., LeBeau, F. E. N., Gillies, M. J., Gillies, M. G., … Racca, C. (2006). Region-specific reduction in entorhinal gamma oscillations and parvalbumin-immunoreactive neurons in animal models of psychiatric illness. *Journal of Neuroscience*, *26*, 2767–2776.

de Curtis, M., & Paré, D. (2004). The rhinal cortices: A wall of inhibition between the neocortex and the hippocampus. *Progress in Neurobiology*, *74*, 101–110.

Deacon, T. W., Eichenbaum, H., Rosenberg, P., & Eckmann, K. W. (1983). Afferent connections of the perirhinal cortex in the rat. *Journal of Comparative Neurology*, *220*, 168–190.

Eichenbaum, H., Sauvage, M., Fortin, N., Komorowski, R., & Lipton, P. (2012). Towards a functional organization of episodic memory in the medial temporal lobe. *Neuroscience & Biobehavioral Reviews*, *36*, 1597–1608.

Faulkner, B., & Brown, T. H. (1999). Morphology and physiology of neurons in the rat perirhinal-lateral amygdala area. *Journal of Comparative Neurology*, *411*, 613–642.

Fuchs, E. C., Neitz, A., Pinna, R., Melzer, S., Caputi, A., & Monyer, H. (2016). Local and distant input controlling excitation in layer II of the medial entorhinal cortex. *Neuron*, *89*, 194–208.

Gnatkovsky, V., & de Curtis, M. (2006). Hippocampus-mediated activation of superficial and deep layer neurons in the medial entorhinal cortex of the isolated guinea pig brain. *Journal of Neuroscience*, *26*, 873–881.

Hamam, B. N., Amaral, D. G., & Alonso, A. A. (2002). Morphological and electrophysiological characteristics of layer V neurons of the rat lateral entorhinal cortex. *Journal of Comparative Neurology*, *451*, 45–61.

Hippenmeyer, S., Vrieseling, E., Sigrist, M., Portmann, T., Laengle, C., Ladle, D. R., & Arber, S. (2005). A developmental switch in the response of DRG neurons to ETS transcription factor signaling. *PLoS Biology*, *3*, e159.

Ikegaya, Y., Sasaki, T., Ishikawa, D., Honma, N., Tao, K., Takahashi, N., … Matsuki, N. (2013). Interpyramid spike transmission stabilizes the sparseness of recurrent network activity. *Cerebral Cortex*, *23*, 293–304.

Jiang, X., Shen, S., Cadwell, C. R., Berens, P., Sinz, F., Ecker, A. S., … Tolias, A. S. (2015). Principles of connectivity among morphologically defined cell types in adult neocortex. *Science*, *350*, aac9462.

Klausberger, T., & Somogyi, P. (2008). Neuronal diversity and temporal dynamics: The unity of hippocampal circuit operations. *Science*, *321*, 53–57.

Koganezawa, N., Taguchi, A., Tominaga, T., Ohara, S., Tsutsui, K.-I., Witter, M. P., & Iijima, T. (2008). Significance of the deep layers of entorhinal cortex for transfer of both perirhinal and amygdala inputs to the hippocampus. *Neuroscience Research*, *61*, 172–181.

Kubota, Y., Karube, F., Nomura, M., & Kawaguchi, Y. (2016). The diversity of cortical inhibitory synapses. *Frontiers in Neural Circuits*, *10*, 27.

Kuchibhotla, K. V., Gill, J. V., Lindsay, G. W., Papadoyannis, E. S., Field, R. E., Sten, T. A. H., … Froemke, R. C. (2016). Parallel processing by cortical inhibition enables context-dependent behavior. *Nature Neuroscience*, *20*, *62–71*.

Kumar, S. S., & Buckmaster, P. S. (2006). Hyperexcitability, interneurons, and loss of GABAergic synapses in entorhinal cortex in a model of temporal lobe epilepsy. *Journal of Neuroscience*, *26*, 4613–4623.

Madisen, L., Mao, T., Koch, H., Zhuo, J. M., Berenyi, A., Fujisawa, S., … Zeng, H. (2012). A toolbox of Cre-dependent optogenetic transgenic mice for light-induced activation and silencing. *Nature Neuroscience*, *15*, 793–802. doi: 10.1038/nn.3078.

Markram, H., Toledo-Rodriguez, M., Wang, Y., Gupta, A., Silberberg, G., & Wu, C. (2004). Interneurons of the neocortical inhibitory system. *Nature Reviews Neuroscience*, *5*, 793–807.

Martina, M., Royer, S., & Paré, D. (2001). Propagation of neocortical inputs in the perirhinal cortex. *Journal of Neuroscience*, *21*, 2878–2888.

Mathiasen, M. L., Hansen, L., & Witter, M. P. (2015). Insular projections to the parahippocampal region in the rat. *Journal of Comparative Neurology*, *523*, *1379–1398*.

Melzer, S., Michael, M., Caputi, A., Eliava, M., Fuchs, E. C., Whittington, M. A., & Monyer, H. (2012). Long-range-projecting GABAergic neurons modulate inhibition in hippocampus and entorhinal cortex. *Science*, *335*, 1506–1510.

Miles, R. (1990). Synaptic excitation of inhibitory cells by single CA3 hippocampal pyramidal cells of the guinea-pig in vitro. *The Journal of Physiology*, *428*, 61–77.

Mizuseki, K., & Buzsáki, G. (2013). Preconfigured, skewed distribution of firing rates in the hippocampus and entorhinal cortex. *Cell Reports*, *4*, 1010–1021.

Moyer, J. R., McNay, E. C., & Brown, T. H. (2002). Three classes of pyramidal neurons in layer V of rat perirhinal cortex. *Hippocampus*, *12*, 218–234.

Nieuwenhuys, R. (2012). The insular cortex: A review. *Progress in Brain Research*, *195*, 123–163.

Paxinos, G., & Franklin, K. (2001). *The mouse brain atlas in stereotaxic coordinates*. San Diego, CA: Academic.

Pelletier, J. G., Apergis, J., & Paré, D. (2004). Low-probability transmission of neocortical and entorhinal impulses through the perirhinal cortex. *Journal of Neurophysiology*, *91*, 2079–2089.

Pennartz, C. M. A., Uylings, H. B. M., Barnes, C. A., & McNaughton, B. L. (2002). Memory reactivation and consolidation during sleep: From cellular mechanisms to human performance. In *Progress in Brain Research* (Vol. *138*, pp. 143–166). Amsterdam, Netherlands: Elsevier.

Pfeffer, C. K., Xue, M., He, M., Huang, Z. J., & Scanziani, M. (2013). Inhibition of inhibition in visual cortex: The logic of connections between molecularly distinct interneurons. *Nature Neuroscience*, *16*, 1068–1076.

Pinto, A., Fuentes, C., & Paré, D. (2006). Feedforward inhibition regulates perirhinal transmission of neocortical inputs to the entorhinal cortex: Ultrastructural study in guinea pigs. *Journal of Comparative Neurology*, *495*, 722–734.

Purves, D., Augustine, G. J., Fitzpatrick, D., Katz, L. C., LaMantia, A.-S., McNamara, J. O., & Mark Williams, S. (2001). *Excitatory and inhibitory postsynaptic potentials*. Sunderland, MA: Sinauer Associates.

Puzerey, P. A., & Galán, R. F. (2014). On how correlations between excitatory and inhibitory synaptic inputs maximize the information rate of neuronal firing. *Frontiers in Computational Neuroscience*, *8*, 59.

Ruth, R. E., Collier, T. J., & Routtenberg, A. (1988). Topographical relationship between the entorhinal cortex and the septotemporal axis of the dentate gyrus in rats: II. Cells projecting from lateral entorhinal subdivision. *Journal of Comparative Neurology*, *270*, 506–516.

Schindelin, J., Arganda-Carreras, I., Frise, E., Kaynig, V., Longair, M., Pietzsch, T., … Cardona, A. (2012). Fiji: An open-source platform for biological-image analysis. *Nature Methods*, *9*, 676–682.

Schindelin, J., Rueden, C. T., Hiner, M. C., & Eliceiri, K. W. (2015). The ImageJ ecosystem: An open platform for biomedical image analysis. *Molecular Reproduction and Development*, *82*, 518–529.

Sohal, V. S., Zhang, F., Yizhar, O., & Deisseroth, K. (2009). Parvalbumin neurons and gamma rhythms enhance cortical circuit performance. *Nature*, *459*, 698–702.

Somogyi, P., Tamás, G., Lujan, R., & Buhl, E. H. (1998). Salient features of synaptic organisation in the cerebral cortex. *Brain Research. Brain Research Reviews*, *26*, 113–135.

Srinivas, S., Watanabe, T., Lin, C. S., William, C. M., Tanabe, Y., Jessell, T. M., & Costantini, F. (2001). Cre reporter strains produced by targeted insertion of EYFP and ECFP into the ROSA26 locus. *BMC Developmental Biology*, *1*, 4.

van Strien, N. M., Cappaert, N. L. M., & Witter, M. P. (2009). The anatomy of memory: An interactive overview of the parahippocampal-hippocampal network. *Nature Reviews. Neuroscience*, *10*, 272–282.

Suzuki, N., & Bekkers, J. M. (2006). Neural coding by two classes of principal cells in the mouse piriform cortex. *Journal of Neuroscience*, *26*, 11938–11947.

Telfeian, A. E., & Connors, B. W. (2003). Widely integrative properties of layer 5 pyramidal cells support a role for processing of extralaminar synaptic inputs in rat neocortex. *Neuroscience Letters*, *343*, 121–124.

Unal, G., Apergis-Schoute, J., & Paré, D. (2012). Associative properties of the perirhinal network. *Cerebral Cortex*, *22*, 1318–1332.

Unal, G., Pare, J.-F., Smith, Y., & Pare, D. (2013). Differential connectivity of short- VS. long-range extrinsic and intrinsic cortical inputs to perirhinal neurons. *Journal of Comparative Neurology*, *2550*, 2538–2550.

de Villers-Sidani, E., Tahvildari, B., & Alonso, A. (2004). Synaptic activation patterns of the perirhinal-entorhinal inter-connections. *Neuroscience*, *129*, 255–265.

Willems, J. G. P., Wadman, W. J., & Cappaert, N. L. M. (2016). Distinct spatiotemporal activation patterns of the perirhinal-entorhinal network in response to cortical and amygdala input. *Frontiers in Neural Circuits*, *10*, 44.

Witter, M. P. (1993). Organization of the entorhinal—Hippocampal system: A review of current anatomical data. *Hippocampus*, *3*, 33–44.

Witter, M. P., Groenewegen, H. J., Lopes da Silva, F. H., & Lohman, A. H. (1989). Functional organization of the extrinsic and intrinsic circuitry of the parahippocampal region. *Progress in Neurobiology*, *33*, 161–253.

Wouterlood, F. G., Härtig, W., Brückner, G., & Witter, M. P. (1995). Parvalbumin-immunoreactive neurons in the entorhinal cortex of the rat: Localization, morphology, connectivity and ultrastructure. *Journal of Neurocytology*, *24*, 135–153.

Zeldenrust, F., Chameau, P. J. P., & Wadman, W. J. (2013). Reliability of spike and burst firing in thalamocortical relay cells. *Journal of Computational Neuroscience*, *35*, 317–334.

SUPPORTING INFORMATION

Additional Supporting Information may be found online in the supporting information tab for this article.

How to cite this article: Willems JGP, Wadman WJ, Cappaert NLM. Parvalbumin interneuron mediated feedforward inhibition controls signal output in the deep layers of the perirhinal-entorhinal cortex. *Hippocampus*. 2018;28:281–296. https://doi.org/10.1002/hipo.22830